JOURNAL OF MECHANICAL ENGINEERING AND SCIENCES (JMES)
ISSN: 2289-4659 e-ISSN: 2231-8380
VOL. 16, ISSUE 1, 8754 – 8769
DOI: https://doi.org/10.15282/jmes.16.1.2022.09.0692

ORIGINAL ARTICLE

Development of non-linear models to evaluate the NiTi SMA spring actuator

D. Singh[1], R. Choudhury[1], M. Mukherjee[2], Y. Singh[1]

[1] Department of Mechanical Engineering, National Institute of Technology Silchar, Assam, Pin-788010, India
Phone: +91 9854149839
[2] Advanced Manufacturing Centre, CSIR-Central Mechanical Engineering Research Institute, Durgapur, West Bengal, Pin-713209, India

ABSTRACT – The shape memory alloy (SMA) based actuators are replacing huge and bulky actuators because of its ability to provide high work per unit mass and serves as active prismatic joint to develop precise robotic manipulators. It also helps in developing a light weight manipulators with a simple actuation process. Here, the study presents the relationship between the contraction of Nitinol SMA prings and the input variables such as current and time to effectively interpret the behavioural complexity. In addition, the response of two Shape memory alloy springs in series combination has been discussed. The finite element analysis (FEA) of the SMA wire and spring has also been carried out to predict the fatigue life of SMA wire and spring. The result showed that the contraction rate of SMA spring increases with increase in current and vice-versa. Moreover, the range of current is classified based on its significance. The relationship of current, displacement and time parameters, during the actuation of SMA spring, is a second order polynomial regression model. The applied current and time have positive impact on the contractiong rate of SMA. Several polynomial regression models were developed in order to predict the precise amount of spring actuation. This study also predicts the range of current suitable for its actuation based on its application as actuator. The FEA result shows that the SMA springs can have high endurance stress limit which makes it unique as compared to other commercially available actuators. This study enables to predict the rate of contraction and the deflection trend of SMA based actuators for precise positioning applications.

ARTICLE HISTORY
Received: 19th Oct. 2020
Revised: 21st Sept. 2021
Accepted: 01st Dec. 2021

KEYWORDS
NiTi spring;
shape memory alloy;
rate of contraction;
non-linear model;
fatigue life

INTRODUCTION

Smart materials are currently in high demand in varied fields due to its remarkable ability to change the structure in response to outside factors such as stress, temperature, electric and magnetic fields [1]. The actuation behaviour of one of the smart materials i.e. Ni-Ti alloy is outstanding and gaining huge importance in various fields including robotics and mechatronics. Robotics is one of the advanced technologies where huge research on the application of smart materials is being carried out from the last few years.

Ni-Ti alloy is a smart material. When deformed, it can restore to its memorized shape under thermal loading due to the variation in crystal orientation from the monoclinic (martensite phase) to the BCC (body centred cubic) structure (austenite phase). Since nitinol contracts in the presence of adequate heat, it is termed as a Shape Memory Alloy. SMA provides high power per unit mass compared to the other conventional actuators, as discussed in Table 1 [2].

Table 1. Power density versus mass of various actuators [2]

Types of actuator	Actuators	Mass (kg)	Power/mass ratio (W/kg)
Conventional actuators	Electric motor	0.1 to 100	10 to 50
	Hydraulic devices	10 to 1000	1000
Smart actuators	Shape memory alloy	0.05	230

The table indicates that SMA possesses approximately five times higher power/mass ratio than the conventional electrical motors. Also, the mass of hydraulic devices like hydraulic linear actuators are very high and hence its comparison with SMA is irrelevant. Also, the SMA is very light in weight and undergoes silent actuation [3]. Variation in temperature of the SMA leads to change in its shape, location, natural frequency, stiffness and other mechanical properties. Because of such unique mechanical properties, the SMA is being researched and used for many applications such as commercial, biomedical, aerospace industries, etc., with one of its primary applications as actuators [4]. SMA actuators are demanding immense popularity as it is a very minute and compact actuator with a larger power/mass ratio, silent operation, low voltage activation and most importantly, biocompatibility [4]. Nitinol, a 50% Ni and 50% Ti SMA, exhibits one of the fundamental characteristics called super-elasticity, enabling it to recover even large strain under certain isothermal conditions [5]. There are many studies on SMA based actuators for different applications like the design of

*CORRESPONDING AUTHOR | D. Singh | ✉ deepsingh.0318@gmail.com

prosthetic hand using two SMA actuators was introduced by Chee Siong et al. [6]. A robotic fish was designed by Tao et al. based on the idea of an FSMA hybrid mechanism with a caudal peduncle actuator which has a fast response and strong thrust ability [7]. BATMAV [8], [9] and Bat Robot [10] are a few flying robots developed using SMA. Also, Festo Group developed a dragonfly having 44 cm in length and a wingspan of 63 cm. Four SMA actuators controls the motion. It has 13 degrees of freedom and is also known as BionicOpter which can fly in mid-air and manoeuvre in multi-directions [11]. Passive microgrippers were developed by Mohammed Ali and Takhata with a RF magnetic field and has wireless actuation capability [12]. SMA wires were implemented to develop bidirectional rotating actuators using open and closed-loop control schemes and investigated mechanical, electrical and thermal characteristics for actuator characterization [13]. A rotational actuator using an SMA spring has been developed in which SMA displaces a rocker arm induces rotational motion to the drive shaft by displacement of the rocker arm. The result showed a peak torque of 1.72 Nm and a relatively smooth motion [14]. Variable Geometry Chevron (VGC), an active serrated aerodynamic device using SMA actuators, has been developed and is installed in the GE90-115B. It minimises noise during takeoff by increasing chevron deflection and improves cruise efficiency by decreasing chevron deflection [15–17]. Sofla et al. [18] developed a shape morphing wing design for small aircraft by applying SMA-actuated flexural structural forms which helps in varying the profile of the wing by bending and twisting to increase the aerodynamic efficiency. Icardi and Ferero also investigated that an adaptable wing on a small unmanned aircraft actuated by SMA devices could bear aerodynamic pressure in any flight condition without adding weight or reducing rigidity [19]. SMAs are utilised in spacecraft for low-shock release mechanisms as they can be operated slowly by progressive heating and can absorb vibration. It can also be developed in a compact and simple design which serves the purpose for the average and smaller sized aircrafts such as micro-satellite [20–22]. Recently, the SMA actuator was used to develop the seventh-generation Chevrolet Corvette vehicle in order to actuate the hatchvent, which helps in easy closing of the trunk lid by releasing air from the trunk [23]. SMAs are also used in future technologies such as electric generators for the electric generation from exhaust heat. It also controls the ow of air in the engine compartment. It also helps reduce aerodynamic drag at high speeds and is also used in the adaptive handle mechanism for opening the vehicle door [24]. In the reference [3], the researchers presented the inverse and forward kinematics along with the workspace of the three-legged U-shaped base PRP-PRP-PRP planar robotic manipulator experimentally by implementing the SMA nitinol as an actuator by joule heating.

The U.S. Naval Ordnance Laboratory discovered a new material that exhibited shape memory effect. Hence, the material or the alloy was named as nitinol (Nickel Titanium Naval Ordnance Laboratory). Nitinol, a superelasticity alloy, helps the SMAs to recover even considerable strain under certain isothermal conditions [5]. The composition of nitinol is 50% Nickel and 50%Titanium. On heating, the shape memory alloys above the austenite finish temperature recover the deformation undergone due to applied stress [25]. With the increase in applied stress, the displacement also increases for the nitinol SMA actuator. Also, the actuation displacement rises with an increase in winding angle [26].

However, one of the key disadvantages of NiTi SMA is hysteresis, which complicates the displacement control due to its continual non-linear change in length, especially when micro-motion is taken into account [4].

Singh et al. analysed the workspace of the three-limb U-shape base 3PRP planar parallel robotic mechanism, as depicted in Figure 1, experimentally by implementing nitinol SMA spring as the actuator [3]. The nitinol spring was actuated by joule heating. The end-effector position and the workspace of the manipulator were determined based on open-loop condition of the actuator. It has two options: ON or OFF. The actuation was performed in order to fully contract the nitinol in the manipulator's limb. The simple ON/OFF actuation system seemed incompatible for accurate and precise end-effector motion. Also, a closed feedback system is necessary to automate the process for the end-effector to travel the designated path. Singh et al. [27, 28] also presented the workspace associated with the different U-shaped manipulators of its family.

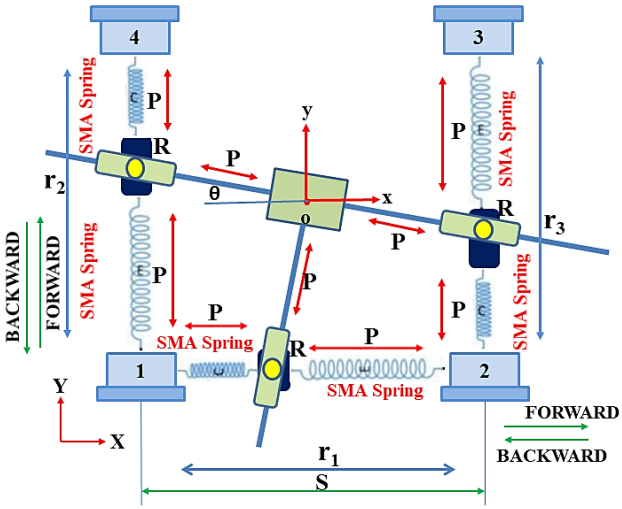

Figure 1. Schematic figure of 3PRP manipulator

Each of the three legs of the manipulator, in Figure 1, consists of two springs which under contraction provides bidirectional motion to the active prismatic joints. The motion of the active prismatic joints varies the position of the end-

effector. The end-effector orientation of the manipulator is dependent upon the actuators position and the precision depends upon its velocity. Hence, to position the end-effector precisely, the spring joints (5, 6, 7), in Figure 1, should be precisely positioned at the desired location based on inverse kinematics. As the supply of electric current actuates the nitinol spring, its contraction depends upon the parameters current and the time duration for which the current is supplied. Hence, such manipulator demands the mathematical model to determine the displacement (or the contraction) of the nitinol SMA spring in terms of current and time.

There are only few articles available on the control of micro-displacement ofthe NiTi SMA actuators. Furthermore, the majority of the research is focused on the SMA wire and its macro-mechanism. The displacement response of SMA springs under joule heating conditions is merely presented. From the previous work on SMA wire and other available SMA actuators, there is a lot of scope for its study and analysis for the micro-motion behaviour of such SMA spring-based actuators concerning time and current.

Therefore, to further comprehend the behavioural complexity, the relationship between the contraction of the nitinol spring with respect to the time and current as input variables has been evaluated in this study. Also, the series connection response of the SMA springs has been investigated. The FEA analysis of the SMA wire and spring was carried out to understand and predict the fatigue life. Polynomial regression models were developed in order to predict the precise and accurate micro-positioning of the SMA spring. This study also predicts the range of applied current suitable for the purpose of actuation. Furthermore, this model can be implemented to develop a manipulator using the developed mathematical model, which can be programmed for different trajectories.

EXPERIMENTAL PROCEDURE

Material Selection and Specification

The NiTi SMA spring with 19 helix windings and a diameter of 0.75 mm has been selected as the actuation material. The general composition of NiTi is 50 wt% Ni and 50 wt% Ti. The commercial NiTi SMA spring can contract ~ upto 29 mm when cooled and can be expanded or deformed up to 140 mm on the application of 6 N load approximately. These SMA springs can also be used in series to acquire higher displacement and also in parallel for a higher force. NiTi SMA spring has the capacity to attain a maximum deformation of up to 8%, which is maximum as compared to other SMA materials [25], [29].

Table 2. Components for variable DC power supply

Component	Details	Quantity
LM317T	Adjustable linear voltage regulator	1
BT139	NPN transistor	1
2SD1047	Transistor to control the current flow	1
	220 ohms	1
Resistors	4000 ohm - 7 Watt	1
	4.7 ohm - 10W	1
Potentiometers	10 kohm	2
LED	monochrome	1
Wires	copper	1
Breadboard	Non-soldering circuit board	1
AC/DC Adapter	Input: 100-240 V, 50/60 Hz, 1.6 A; Output: 15 V, 5 A	1

In order to actuate the NiTi SMA spring, the temperature of the spring has to be elevated up to the austenite phase of the material in order to undergo phase conversion. The phase transformation is carried out with the help of either joule heating or any other heating process. In this present work, the temperature of the SMA springs are elevated by allowing through the current across the terminals, which in thereby increases the temperature of the springs (due to the internal resistance), resulting in phase transformation. To provide the variable DC, a variable current DC power supply using several components, as listed in Table 2, has been developed. The electrical current that leads to thermal loading on the nitinol spring needs to be studied as it correlates to its contraction. Higher the electrical current, faster the spring contracts and vice-versa. Hence, the correlation between the electrical current and contraction time and length is the key to forecast the actuation displacement. The minimum current deviation obtained in the DC variable power supply is 10 mA. The schematic circuit diagram for the DC variable power supply is depicted in Figure 2(a). The actual variable DC power supply utilised in the study is presented in Figure 2(b).

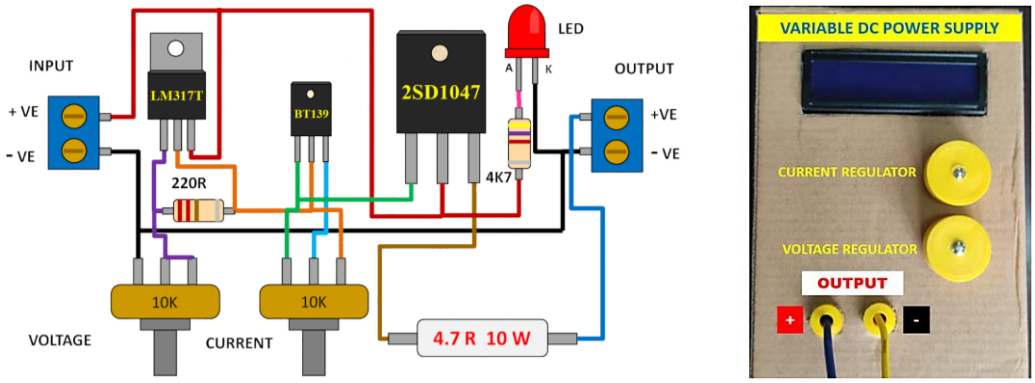

(a) (b)

Figure 2. Variable DC power supply: (a) Circuit diagram and (b) Fabricated Prototype

SolidWorks Model

The CAD model for the Nitinol wire and the spring has been modelled in SolidWorks 2016 software to carry out the finite element analysis by using the Ansys Workbench 18.1. The 2D drawings of the computer aided designed wire and the spring has been shown in the Figure 3. The spring has been modelled with 0.75 mm as wire diameter with 10 helical windings.

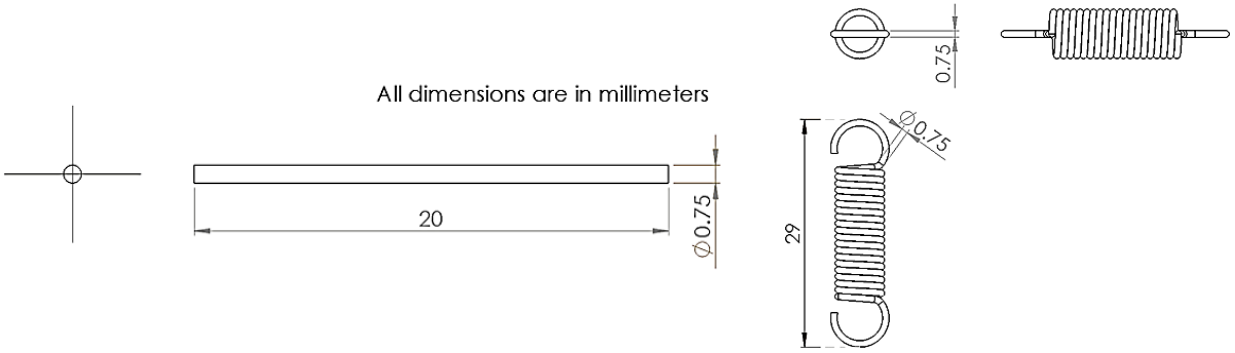

(a) (b)

Figure 3. (a) Nitinol wire (b) Nitinol spring with 10 helical windings

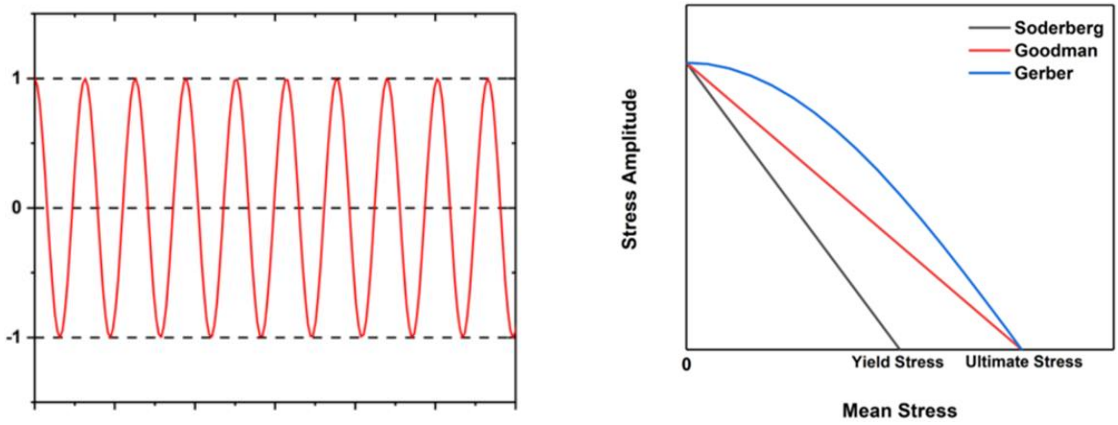

(a) (b)

Figure 4. (a) Constant amplitude load fully reversed and (b) Mean stress correction theory

To understand the fatigue life of the NiTi SMA, an FEA based fatigue analysis of a 0.75 mm diameter wire was modelled initially and then the result of the model was further implemented on the NiTi SMA spring model. The various input parameters [30], [31] that have been taken into consideration in order to carry out the FEA analysis is given in the Table 3. The static structural analysis of the NiTi SMA wire and spring was carried out using the SolidWorks 2016 CAD Model shown in Figure 3 by imposing the properties as shown in Table 3. The super-elasticity properties of the Nitinol SMA have been taken into consideration. The application of load is fully reversed (i.e. R = -1) and the Soderberg's mean stress theory has been taken into consideration, as depicted in the Figure 4, with the σ_Y value of the NiTi alloy.

The SolidWorks CAD Model of the wire and spring was imported into Ansys Workbench and the static structural test was selected. The parameters of the Nitinol were imported into the engineering material database which has been shown in Table 3. The default coarse mesh was implied in the model and the meshed model characteristics for the wire was 3986 nodes and 748 elements and that for the spring was 36814 nodes and 6974 elements. To undergo the analysis, various load values were applied at one end of the wire by providing fixed support at the other end. Also, the 'Large Deflection' was activated to achieve real-time structural property. On changing the load values and performing the analysis various parameters such as maximum principal stress, maximum principal strain, total deformation, normal stress and fatigue life was noted without strain convergence and with 8% strain convergence.

Table 3. Properties of Nitinol [30,31]

Type of property	Properties	Value	
Physical property	Density	6.45 g/cm^3	
	Temperature	22^{0}C	
Isotropic elasticity	Young's modulus	70000 MPa	
	Poisson's ratio	0.33	
Strength	Tensile yield strength	559 MPa	
	Compressive yield strength	560 MPa	
	Tensile ultimate strength	960 MPa	
	Compressive ultimate strength	960 MPa	
Super-elasticity	Sigma SAS	52000 psi	
	Sigma FAS	60000 psi	
	Sigma SSA	30000 psi	
	Sigma FSA	20000 psi	
	Epsilon	0.7 in/in	
	Alpha	0.1	
Alternating mean stress	Stress (for log-log interpolation)	Cycles	Alternating stress (Pa)
		1000	550
		5000	520
		10000	450
		100000	430
		1000000	410

SMA Spring in Series Connection

Two NiTi SMA springs were used to study the its behaviour under series arrangement. One end of first spring was locked at the origin (0, 0) and one of the ends of second spring was locked at location B (l, 0) where, l = 129 mm. As shown in Figure 5, the other end of the two SMA springs is linked together at point A (r, 0) with the aid of an ABS plastic pin printed using FDM 360 mc fused deposition modelling machine. Initially current is supplied to the second spring and the spring gets contracted due to the temperature rise. After contraction, the current is switched off. The spring is allowed to cool down to room temperature. The first spring is supplied with a constant current and the location of A is determined and recorded every 10 seconds.Similarly, the position of A was established by supplying different values of constant current to the spring using the developed variable DC power supply.

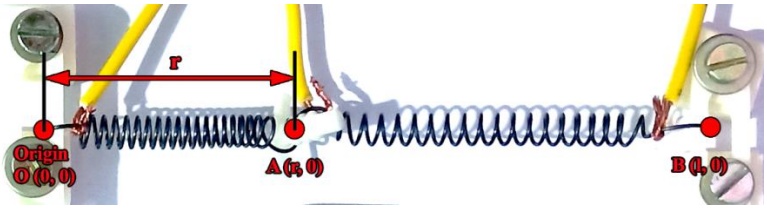

Figure 5. Series connection of NiTi SMA spring

Mathematical Models

Several non-linear mathematical models were developed to understand the complex deflection behaviour of the NiTi SMA spring. The development of the mathematical models has been divided into two parts: 1) development of non-linear models for single spring connection and 2) development of non-linear models for series connection of two springs. The

current and the time of contraction of the spring are considered as the input variables in the models. The deflection or deformation of the spring after constant time interval was measured at different current amplitudes and considered as the response parameter of the models. Two types of model are used in the study to understand the response and variable relationships for different configurations. The non-linear exponential models were developed to realise the one-to-one relationship between response and variable for individual spring connection. The generalized non-linear exponential mathematical model can be represented by the Eq. (1).

$$d = d_0 + a \times e^{bt} \tag{1}$$

where d is displacement, t is time and d_0, a and b are constant coefficients.

Similarly, multivariable correlations were depicted by adopting a second-order quadratic polynomial model. The generalized second-order relationship for the deflection response as a function of time and current is given in Eq. (2).

$$d = a_0 + a_1 \times t + a_2 \times I + a_{11} \times t^2 + a_{22} \times I^2 + a_{12} \times t \times I \tag{2}$$

where a_0, a_1, a_2, a_{11}, a_{22}, a_{12} being the coefficients.

RESULTS AND DISCUSSION

Determination of Current-Time Domain for Single Spring Connection

In this paper, an attempt has been made to control the displacement of the shape memory alloy spring so that it can efficiently be utilised as a smart linear actuator in the micron level. In the experiment, the SMA spring contracts, in the presence of electrical current, from its original stretched length (L_0) of 100 mm. The Ohm's law shows that for a fixed current if time increases energy also increases and vice-versa. This is applied in this study where the current is fixed at a particular value (with a specified tolerance) and the contraction time was recorded for a standard contraction length (L_c) of 71 mm. The details of the selected and obtained parameters are given in Table 4.

Table 4. Experimental data for current vs time for full contraction

Sl. No.	Current, I (mA)	Initial Length, L_0 (mm)	Final Length, L_f (mm)	Contraction Length, L_c(mm)	Time, t (sec)	Remark's
1	1220	100	29	71	72.4	Rapid actuation
2	1150	100	29	71	84.4	
3	1100	100	29	71	100	
4	1080	100	29	71	101.7	
5	1030	100	29	71	153.7	Fast actuation & Low precision
6	1000	100	29	71	169	
7	950	100	29	71	180	
8	930	100	29	71	262	
9	900	100	29	71	300	Slow actuation & High Precision
10	850	100	29	71	358.6	
11	810	100	29	71	393.5	
12	800	100	29	71	420	
13	750	100	29	71	570.8	
14	700	100	29	71	626.8	
15	600	100	50.75	49.25	5460	Infeasible

The current was altered from 600 mA to 1220 mA in 15 steps during the experiment to determine the total deflection time necessary to reach L_c. The results showed that the entire current range can be divided into four different groups according to the performance revealed. Therefore, the four categories are (i) rapid actuation, (ii) fast actuation & low precision, (iii) slow actuation & high precision and (iv) infeasible. The first category where the applied current was within the range of 1080 mA to 1220 mA, the time taken for contracting up to final length (L_f) was significantly lower, ranging between 101.7 sec to 72.4 sec which reflects the rapid contraction state of the SMA spring. In this state, it is difficult to manoeuvre the SMA spring in the micron level to develop a micro-motion linear actuator. However, for rapid movement, this stage is applicable where large deflection is significant and instantly needed. The current below 1080 mA and up to 930 mA falls within the second category where the time required for the contraction was comparatively higher than the

first category. Hence, in this case fast actuation is possible with comparatively lower precision. This stage can be applied where the precise measurement is not significant. Furthermore, the current below 930 mA and up to 700 mA falls within the third category where the time required for the contraction was much higher than the second category which signifies high precision, but at the cost of slow actuation. This slow actuation and high precision are probably the most suitable domain for micro-motion linear actuation where the SMA spring deflection can be easily controlled up to micro-level. Beyond this category, where the current falls below 700 mA, the actuation of spring stops at the halfway of the L_c. Therefore, very low current cannot be utilized in the application because of the non-feasibility of complete deflection over time. Alternatively, it can be concluded that the contraction rate from 0.5917 to 1.1833 mm/sec is considered a rapid actuation stage. The contraction rate from 0.2367 to 0.5917 mm/sec is considered as fast actuation stage. Similarly, the contraction rate from 0.1075 to 0.2367 mm/sec is considered as slow/micro actuation. The contraction rate below 0.1075 mm/sec is referred as an infeasible region.

From Table 4, it is observed that there is a correlation between current and time for constant deflection. The development of mathematical modelling can predict correlations. The following sections discuss the non-linear correlations between response (deflection, *d*) and variables (current, *I* and time, *t*) by developing an exponential and second-order quadratic polynomial model respectively.

Non-Linear Exponential Models for Single Spring

The NiTi SMA spring was elongated to an initial length of 100 mm by applying uniaxial force. The experiment was conducted by passing different currents and the time required to reach L_f was noted. The collected data sets were used to develop a fitting correlation between current and time which is plotted in Figure 6.

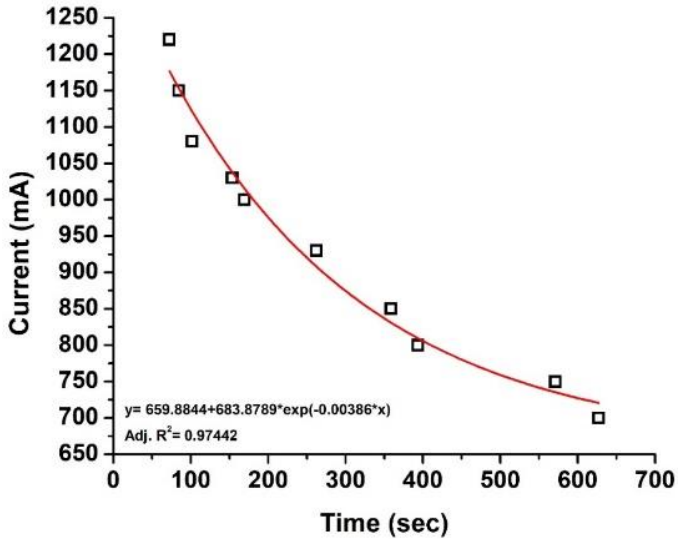

Figure 6. Current (mA) vs time (s) non-linear exponential plot

Figure 6 presents an exponential curve with a negative gradient. This signifies that as the current increases, the time necessary for the same length of contraction (L_c) of SMA spring decreases.The slope is steeper at first and declines progressively indicating that the contraction rate is more prominent for high current than low current values. Also, with further increase in time, the slope will become parallel to the time axis which signifies zero contraction rate below certain current value resulting in no change in length. The plot can be considered in order to quantify the time to be necessary for full contraction (L_f) at any given current. Based on the data in Table 4, a non-linear exponential mathematical model was obtained for the current response with variable parameters as time for full contraction to 29 mm which is given in Eq. (3). The equation depicts a negative exponential coefficient, which clearly indicates that for a given contraction length, more time is needed at lower applied current, which has exponential correlations. The non-linear exponential fitted equation has a step regression value of 0.97442, which signifies that the suitability of the equation with approximately 97.442% fit.

$$I = 659.8844 + 683.8789 \times \exp(-0.00386 \times t) \quad (3)$$

Figure 7(a) shows the real-time picture of variation of the NiTi SMA spring length with time when a constant current of 950 mA was supplied. It can be seen that the length of the SMA spring contracts gradually at a constant current supplied with respect to time. Similar behaviour of SMA spring was also obtained in other current conditions where time taken to reach L_f is different. Figure 7(b) shows the deflection curve with respect to time for different constant current values. It can also be seen how the curve varies and the time increases while the current value decreases. Also, it can be stated that the slope is reducing with the decrease in current and at a certain value of current, the slope will reduce to zero, thereby referring to no more deflection with an increase in time. The fitted graphs plotted in Figure 8(a) – 8(e) have been obtained

based on the obtained current-time response of the SMA spring test. In each case, the curve was fitted to a non-linear exponential model. The graph gives the deflection as a response with the variable parameter i.e. time. As can be seen from each graph, the fitted line has negative slope, which can be verified from the developed exponential Eqs. (4) – (8). In the equations, the exponential coefficient of individual fit is negative, representing the amount of time required for full contraction from L_0. The obtained Eqs. (4) – (8), have adjusted regression values of 0.99356, 0.99365, 0.99229, 0.99576 and 0.99286 respectively, which indicates the acceptability of equations with a more than 99.229% fit and the obtained fit data is mentioned in Table 5.

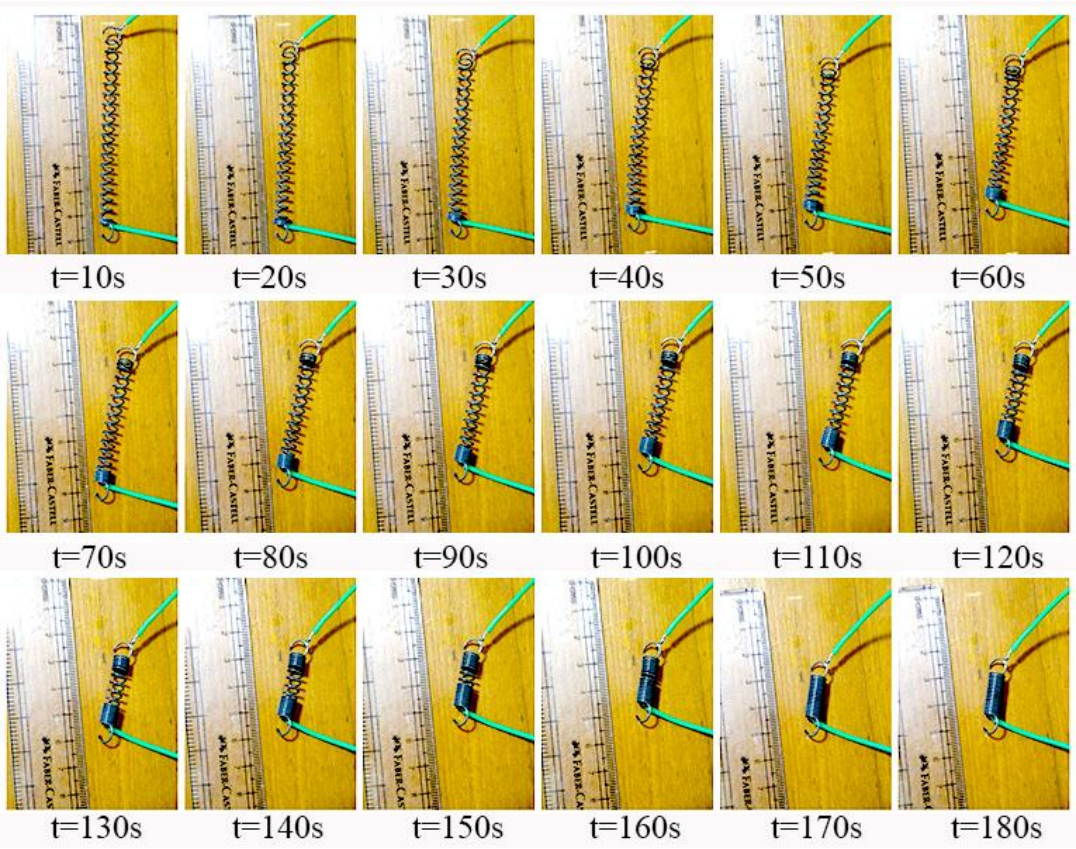

(a)

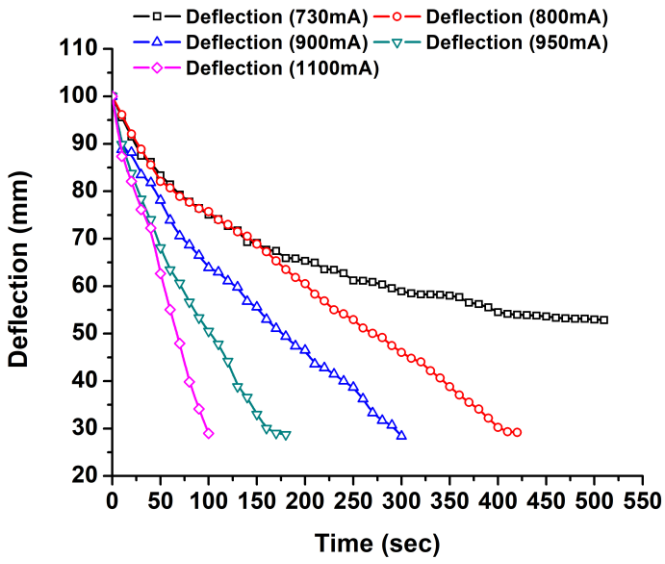

(b)

Figure 7. (a) Real time deflection of NiTi SMA spring at 950 mA current and (b) deflection vs time curve at different constant values of current.

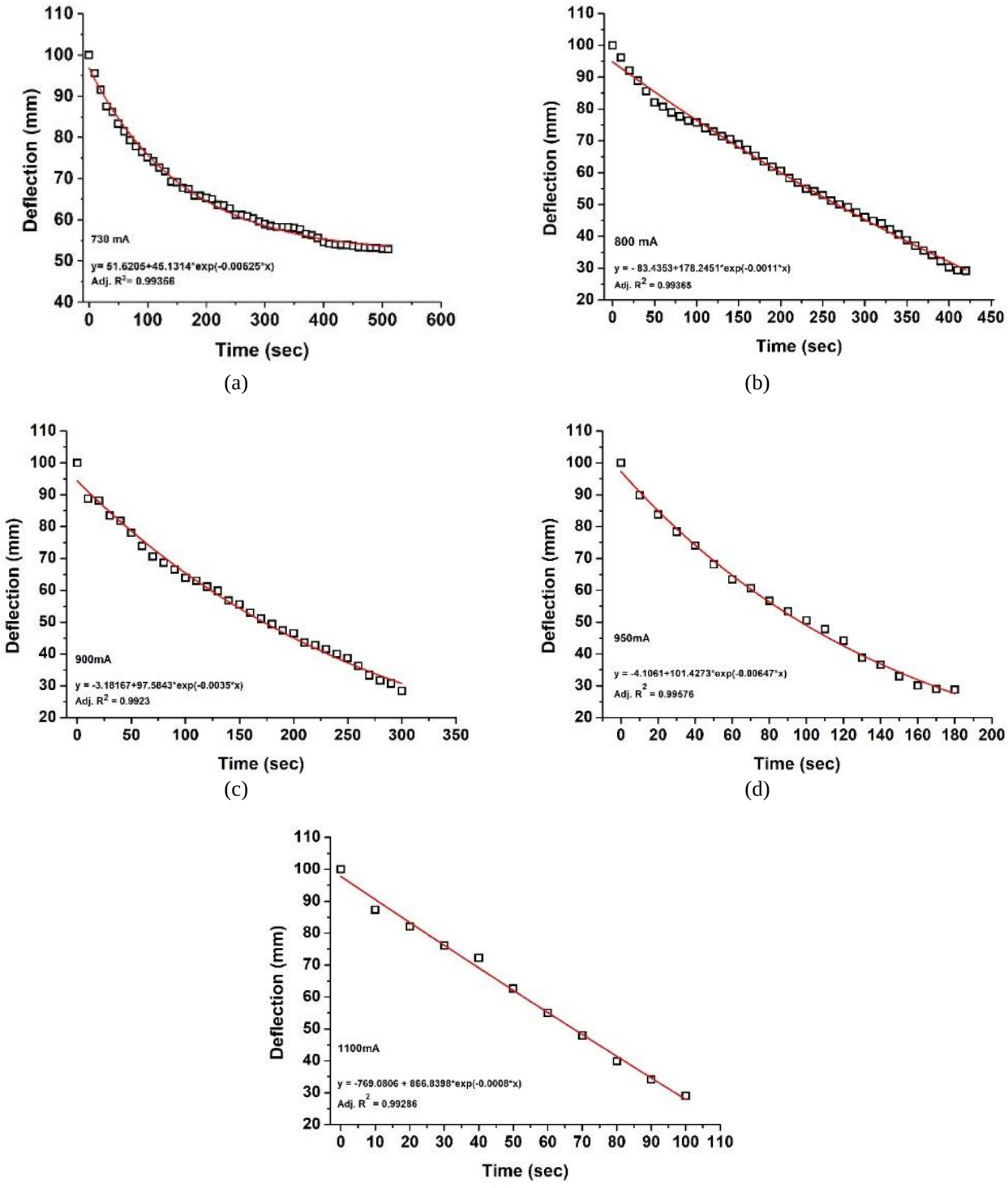

Figure 8. Deflection vs time plots for different activation currents: (a) 730 mA, (b) 800 mA, (c) 900 mA, (d) 950 mA and (e) 1100 mA

Table 5. Statistical fit data for the Eqs. (4) to (8)

Deflection	Coefficients of equation			Statistics	
	d_0	a	b	Reduced Chi-Sqr	Adj. R-Square
Deflection (730 mA)	51.62052	45.1314	-0.006250	0.94696	0.99356
Deflection (800 mA)	-83.4353	178.2451	-0.001090	2.42373	0.99365
Deflection (900 mA)	-3.18167	97.58434	-0.003520	2.85442	0.99229
Deflection (950 mA)	-4.10608	101.4273	-0.006470	1.99865	0.99576
Deflection (1100 mA)	-769.081	866.8399	-0.000840	3.85072	0.99286

The values of each coefficient for the Eqs. (4) – (8) have been provided in Table 5 along with the adjusted regression values.

$$\text{At 730mA, } d = 51.6205 + 45.1314 \times \exp(-0.00625 \times t) \tag{4}$$

$$\text{At 800mA, } d = -83.4353 + 178.2451 \times \exp(-0.0011 \times t) \tag{5}$$

$$\text{At 900mA, } d = -3.18167 + 97.5843 \times \exp(-0.0035 \times t) \tag{6}$$

$$\text{At 950mA, } d = -4.1061 + 101.4273 \times \exp(-0.00647 \times t) \tag{7}$$

$$d = -769.0806 + 866.8398 \times \exp(-0.0008 \times t) \tag{8}$$

Based on the various coefficient data given in Table 5, for various current values, a generalized equation can be derived with the limits of the coefficients as represented in Eq. (9) with an acceptability of 99.43% fit.

$$d = d_0 + a \times \exp(-b \times t) \begin{bmatrix} -769 \le d_0 \le 51 \\ 45 \le a \le 866 \\ 0.00083935 \le d_0 \le 0.00647 \end{bmatrix} \tag{9}$$

Mathematical Model for Deflection Control of Single Spring Connection

Although Eq. (3) and Eq. (9) relate the current-time and deflection-time, respectively, it is not sufficient to correlate all the three parameters. Time should be considered based on the high or low precision requirements and the current will also vary as per productivity.

Table 6. ANOVA for deflection of NiTi spring with respect to the time and current

Source	DF	Seq. SS	Adj. SS	Adj. MS	F-vale	P-value
Regression	5	51340.3	51340.3	10268.1	384.83	0.0001
Linear	2	35021.4	1653.5	826.8	30.99	0.006
t	1	20801.6	1643.9	1643.9	61.61	0.004
I	1	14219.8	483.1	483.1	18.11	0.014
Square	2	11294.3	2027.8	1013.9	38.00	0.002
*t*t*	1	10798.6	1061.6	1061.6	39.79	0.001
*I*I*	1	495.7	609.4	609.4	22.84	0.003
Interaction	1	5024.6	5024.6	5024.6	188.31	0.002
*t*I*	1	5024.6	5024.6	5024.6	188.31	0.001
Residual Error	161	4295.8	4295.8	26.7		
Total	166	55636.1				

Note: According to the probability value, all the variables are significant.

So, a quadratic polynomial model has been formulated for different current values based on current vs time and deflection vs time data. A second-order quadratic polynomial regression model has been used to express the deflection (d) as a function of time (t) and current (I). With a regression value of 0.9204, the following full quadratic polynomial equation is developed. A result of ANOVA for the deflection has been shown in Table 6. Based on the obtained statistical F-value, the deflection response is acceptable because it is unlikely to have a large F-value due to noise. Even the probability value shows a clear indication regarding the importance of the quadratic polynomial equation. The adjusted R^2 value is 0.9204 which is another clear evidence of the sufficiency for the derived quadratic polynomial regression equation for a single spring.

$$d = -30.6349 + 0.4427 \times t + 0.2964 \times I + 0.0002 \times t^2 - 0.0002 \times I^2 - 0.0008 \times t \times I \tag{10}$$

Equation (10) presents the deflection curve or response concerning time and current which are the sole parameters required for the design of the SMA spring-based actuation. Hence, based on any two known parameters, it will be easier to determine the third. Most of the time, the required length of deflection is known and the time can be assumed as per

the productivity and given categories mentioned in Table 6. Hence, the current required for single spring actuation can be predicted from the Eq. (10). This equation serves a vital role to determine the deflection possible for a single NiTi SMA spring at specific values of current and time. It can predict accurately within the domain of experimental data. The range of the various parameters should be within the limits as tabulated in Table 7.

Table 7. Domain of variable parameters

Sl. No.	Parameters	Minimum	Maximum
1	Displacement (mm)	29	100
2	Current (mA)	800	1200
3	Time (s)	0	400
4	Ambient Temperature	Room Temperature	Room Temperature

Predicted Deflection Trend of NiTi SMA Single Spring Connection

As illustrated in Figure 9, the generated quadratic polynomial Eq. (10) provides the deflection variation by presenting the deflection line in a two-dimensional current – time graph.

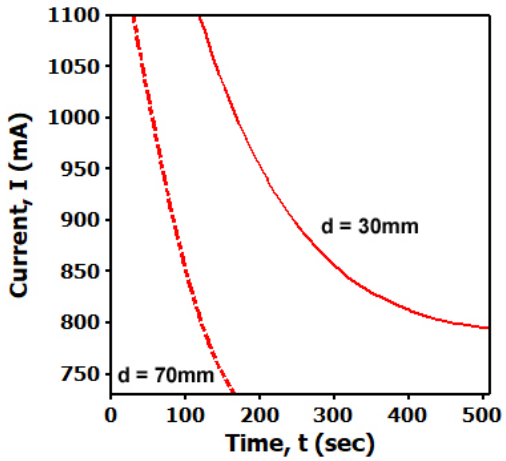

Figure 9. Current vs time graph within deflection range of 30 mm – 70 mm

The figure depicts the deflection variation of limiting displacement as 70 mm and 30 mm. The deflection within this range comes in between. This typical graph gives a clear idea of the total time required for a known current to achieve any deformation. The lines depicting d = 70 mm and d = 30 mm have a negative gradient, indicating that the time required to accomplish any required deflection rises with a drop in current and vice versa. Also, it can be concluded that the gradient of any deflection curve goes on decreasing with a decrease in current. The curve will attain zero slope after a specified amount of time-based on the d = 30 mm line and the time required for the slope to become zero is infinite. Thus no more deflection is possible which shows the infeasibility region as mentioned in Table 4. The current value at this position can be considered as the critical current to start deflection. However, the critical current value varies with the deflection curve, which can easily be figured out based on the d = 30 mm and d = 70 mm lines.

Mathematical Model for Deflection Control of SMA Spring in Series Connection

To achieve micro-actuation with two-axis movement, two shape memory alloy springs were arranged in series with a pin in between, as depicted in Figure 5. The obtained non-linear models (Eqs. (3) to (9)) were used to control the deflection of the springs in series connection as these models are able to describe the single spring deflection suitably. Amazingly, the deformation of the series-joined springs differed from the normal, presumably due to the internal resistance of the springs acting in opposite directions. The deflection response of the series-linked SMA springs could not be interpreted using the equations discussed in the previous sections. As a result, a sequence of experiments were repeated in the same time-current domain, as shown in Table 4. The deflection data of the series connection was obtained for different applied current and the contraction time was recorded. These noted data were used to formulate another 2^{nd} order quadratic polynomial equation similar to a single spring connection.

Table 8. ANOVA for deflection of NiTi spring with respect to time and current for series connection

Source	DF	Seq. SS	Adj. SS	Adj. MS	F-vale	P-value
Regression	5	11369.4	11369.4	2273.87	92.83	0.0001
Residual Error	120	2939.3	2939.3	24.49		
Total	125	14308.7				

Note: According to the probability value, all the variables are significant

The deflection (d_s) of series joined SMA spring has been presented by a 2nd order quadratic polynomial regression model which consists of two process parameters such as time(t) and current(I). The subsequent quadratic polynomial equation is estimated for series connection with a step regression value of 0.8214. A result of ANOVA for the deflection has been shown in Table 8. The quadratic polynomial equation is clearly significant, as indicated by the high F-value and the probability value of smaller than 0.05. The quadratic polynomial function is clearly significant, as evidenced by the high F-value and probability value of less than 0.05. The adjusted R^2 value is 0.8214, which is another clear signal of the sufficiency for the derived quadratic polynomial regression model.

$$d_s = 57.513 - 8.674 \times I - 18.204 \times t - 1.246 \times I^2 + 2.126 \times t^2 - 1.464 \times I \times t \quad (11)$$

Equation (11) dictates the deflection curve or response behaviour concerning the influencing factors, time and current, for a series connection. Based on any two known values, it will be easier to determine the third unknown. Most of the times, the required length of deflection is known and the time can be assumed as per the given categories mention in Table 3. Hence, the required current can be assumed from the Eq. (11).

SMA springs, although being light in weight, provides larger stroke length as compared to conventional actuators. It can be used as actuators to obtain a higher level of accuracy for various applications. The presence of two springs in series also provides bidirectional motion to the joint with an additional advantage of getting a larger stroke length.

The above discussed mathematical models are the key to control the nitinolSMA spring under the discussed limiting operations. The models possess the ability to predict and decide the control parameters such as deflection, current and time for the development of SMA actuators. The developed spring equations can be implemented for various applications including planar parallel manipulators.

Finite Element Analysis (FEA) for the Fatigue of NiTi SMA Wire and Spring

The actuation system is fundamentally a dynamic system where a specific amount of load is applied for a time period and released. This loading-unloading condition has a resemblance to the fatigue condition. Therefore, the fatigue behaviour of SMA springs is necessary to determine the life of the actuator. Estimation of endurance stress is essential for the design of real systems. FEA is an efficient tool to predict the structural fatigue fracture behaviour of the known materials without destructive experiments with adequate accuracy. The properties of the material required to develop a FE model should be known and, in this case, NiTi SMA is a well-known alloy. The properties of NiTi SMA is given in Table 3, which is used in the model. First, the SMA wire of 0.75 mm diameter is considered for the model to generate various parameters such as maximum principal stress, maximum principal strain, total deformation, normal stress and cycles.

Table 9. Ansys data of NiTi SMA spring with 10 windings (with 8% strain convergence)

Force (N)	Total Deformation (mm)	Maximum Principal Elastic Strain (mm/mm)	Maximum Principal Elastic Stress (MPa)	Normal Stress (MPa)	Life (cycles)
5	2.2518	0.0019434	391.01	266.88	1000000
10	4.3319	0.0052176	1029.4	772.1	1000000
15	6.4138	0.0058234	1171.6	842.13	1000000
20	The solver engine was unable to converge on a solution for the nonlinear problem as constrained.				

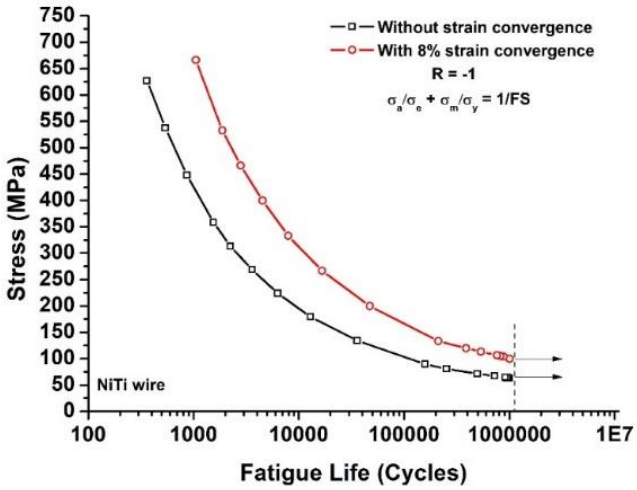

Figure 10. Fatigue life curve of NiTi SMA wire

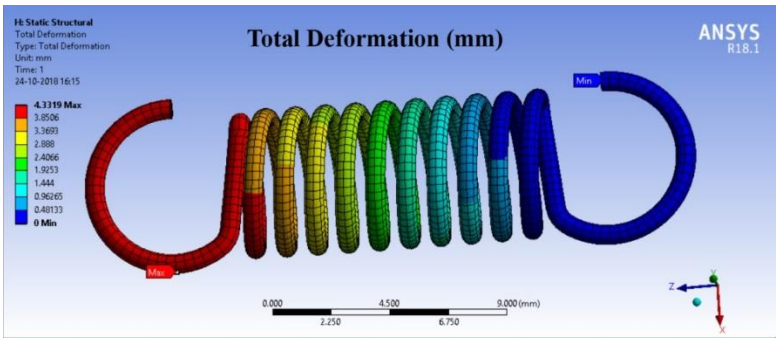

(a)

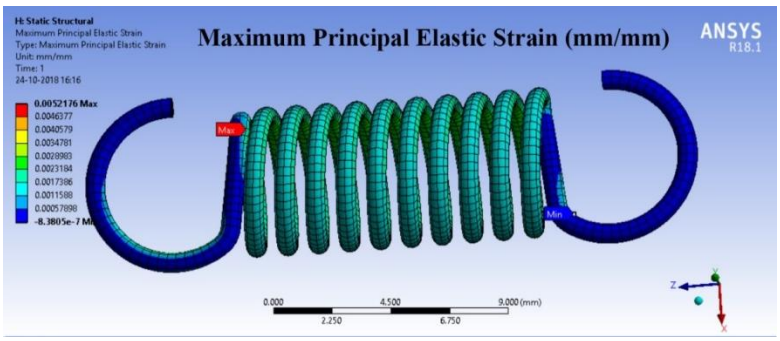

(b)

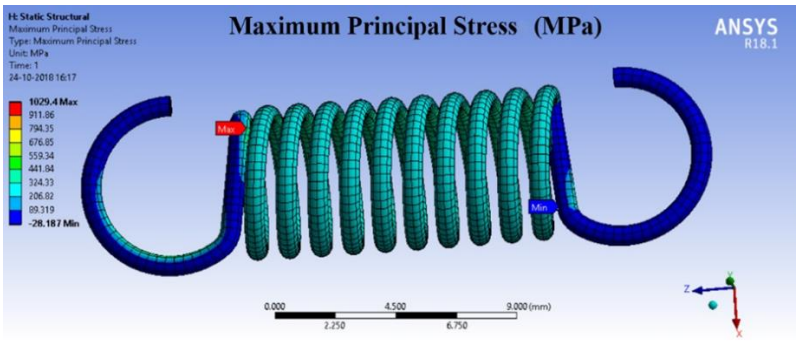

(c)

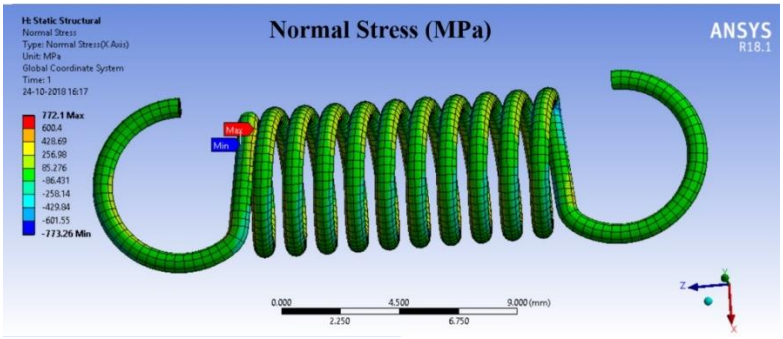

(d)

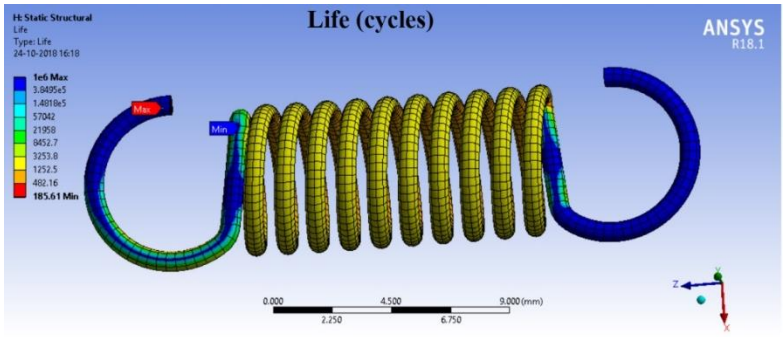

(e)

Figure 11. Ansys model of NiTi SMA spring at 10 N load with 8% strain convergence: (a) Total deformation, (b) Maximum principal elastic strain, (c) Maximum principal stress, (d) Normal stress and (e) Life.

The nominal stress vs cycle, S-N, curves are plotted with and without strain convergence, as shown in Figure 10. The strain convergence of 8% is used in the model because the NiTi has the maximum strain recovery of 8%, beyond which it will not regain its original shape properly. The endurance limit in the S-N curve is generally considered as the stress limit up to 10^6 cycles. It is observed that without strain convergence or in normal conditions, the endurance stress of the wire is ~64 MPa. Correspondingly, the applied load at the endurance limit is ~71 N.

On the other hand, higher endurance limit with endurance stress of ~100 MPa was obtained at a limiting strain convergence of 8%. In this condition, the applied load is about 75 N. Therefore, theoretically, under the application of 70 N load the SMA wire will never fail due to fatigue fracture. These observations and theoretical endurance stress/load of wire were further applied to the spring of the same diameter. The experiment was started with a minimum load of 5 N and the endurance was achieved. Similarly, the load factor was further increased to 10 N and 15 N still, no significant change in endurance was observed. Figure 11 shows the NiTi SMA spring model analysis under a load of 10 N applied at one end by keeping the other end fixed with large deformation. The entire test was conducted under 8% strain convergence condition. The analysed theoretical data of the model is given in Table 9. It is also shown that when the force rises from 15 N to 20 N the solver is unable to converge the solution for the given non-linearity problem.

CONCLUSION

The present study classifies the current range for the SMA spring actuation into four groups based on its significance. The gradient of a regular deflection curve gradually reduces with reducing current over time until it hits critical current, an infeasible area beyond which further contraction is impossible. The deflection vs time plot of the experimental data, at different currents, showed an increase in contraction rate with a rise in current. With rise in current, the rate of contraction of the SMA spring increases and vice versa. It is observed that, for a fixed deflection length, an exponential relation is established between current and time. The developed second-order quadratic polynomial model (a correlation between displacement, current and time) presents the contraction behaviour of the nitinol spring adequately. The polynomial equation can forecast the response effectively as verified by ANOVA. Since the developed single spring polynomial model cannot predict the series connection, another 2nd order polynomial equation was developed to present the deflection response based on the input arguments for the series connected SMA spring. It can predict the response effectively as verified by ANOVA.

The finite element analysis results in significant variation in endurance strength of NiTi SMA wire between 8% strain convergence and no strain convergence with the endurance strength being more in case of 8% strain convergence. Also, FEA of Nitinol springs is inconclusive at higher loads. The developed polynomial regression equations are significantly essential to quantify the deflection trend to develop positioning stages for varied applications.

The study predicts the motion of the nitinol SMA spring based on the developed mathematical models for micro-motion upon linear actuation. These mathematical models are the key to control the NiTi SMA based actuators. It can

also be implemented to develop the planar micro-positioning stage for various applications, including 3D printers, micro-milling machines, micro-drilling machines etc. It can also serve as a stage for the micro-motion of the workpiece within a plane.

ACKNOWLEDGMENTS

The presented work in the paper is supported and funded by CSIR-EMR-II, India (No. 22(0831)/19/EMR-II) and Start-up Research Grant, SERB, DST, India (No. SRG/2020/000491).

REFERENCES

[1] W. G. Drossel, H. Kunze, A. Bucht, L. Weisheit, and K. Pagel, "Smart3 - Smart materials for smart applications," *Procedia CIRP*, vol. 36, pp. 211–216, 2015, doi: 10.1016/j.procir.2015.01.055.

[2] S. Hirose, K. Ikuta, and Y. Umetani, "Development of shape-memory alloy actuators. Performance assessment and introduction of a new composing approach," *Adv. Robot.*, vol. 3, no. 1, pp. 3–16, 1989, doi: 10.1163/156855389X00145.

[3] Y. Singh and S. Mohan, "Development of a planar 3PRP parallel manipulator using shape memory alloy spring based actuators," *ACM Int. Conf. Proceeding Ser.*, vol. Part F1320, pp. 1–6, 2017, doi: 10.1145/3132446.3134874.

[4] L. Miková, S. Medvecká-Beňová, M. Kelemen, F. Trebuňa, and I. Virgala, "Application of shape memory alloy (SMA) as actuator," *Metalurgija*, vol. 54, no. 1, pp. 169–172, 2015.

[5] J. Leng, X. Yan, X. Zhang, M. Qi, Z. Liu, and D. Huang, "A novel bending fatigue test device based on self-excited vibration principle and its application to superelastic Nitinol microwire study," *Smart Mater. Struct.*, vol. 26, no. 10, 2017, doi: 10.1088/1361-665X/aa7bdf.

[6] C. S. Loh, H. Yukoi, and T. Arai, "New shape memory alloy actuator: Design and application in the prosthetic hand," *Annu. Int. Conf. IEEE Eng. Med. Biol. - Proc.*, vol. 7, no. 16360118, pp. 6900–6903, 2005, doi: 10.1109/iembs.2005.1616092.

[7] T. Tao, Y.-C. Liang, and M. Taya, "Bio-inspired actuating system for swimming using shape memory alloy composites," *Int. J. Autom. Comput.*, vol. 3, no. 4, pp. 366–373, 2006, doi: 10.1007/s11633-006-0366-4.

[8] S. J. Furst, G. Bunget, and S. Seelecke, "Design and fabrication of a bat-inspired flapping-flight platform using shape memory alloy muscles and joints," *Smart Mater. Struct.*, vol. 22, no. 1, 2013, doi: 10.1088/0964-1726/22/1/014011.

[9] G. Bunget and S. Seelecke, "Actuator placement for a bio-inspired bone-joint system based on SMA," *Act. Passiv. Smart Struct. Integr. Syst. 2009*, vol. 7288, p. 72880L, 2009, doi: 10.1117/12.816309.

[10] J. Colorado, A. Barrientos, C. Rossi, and K. S. Breuer, "Biomechanics of smart wings in a bat robot: Morphing wings using SMA actuators," *Bioinspiration and Biomimetics*, vol. 7, no. 3, 2012, doi: 10.1088/1748-3182/7/3/036006.

[11] Festo, "Festo Bionic Opter – Inspired by dragonfly flight," 2013. .

[12] M. S. Mohamed Ali and K. Takahata, "Frequency-controlled wireless shape-memory-alloy microactuators integrated using an electroplating bonding process," *Sensors Actuators, A Phys.*, vol. 163, no. 1, pp. 363–372, 2010, doi: 10.1016/j.sna.2010.08.007.

[13] Y. Kim, T. Jang, H. Gurung, N. A. Mansour, B. Ryu, and B. Shin, "Bidirectional rotating actuators using shape memory alloy wires," *Sensors Actuators, A Phys.*, vol. 295, pp. 512–522, 2019, doi: 10.1016/j.sna.2019.05.047.

[14] N. Hofmann and M. P. Hennessey, "Shape memory alloy based rotational actuator," *ASME Int. Mech. Eng. Congr. Expo. Proc.*, vol. 4B-2018, pp. 1–10, 2018, doi: 10.1115/IMECE2018-87646.

[15] S. D. Oehler, D. J. Hartl, R. Lopez, R. J. Malak, and D. C. Lagoudas, "Design optimization and uncertainty analysis of SMA morphing structures," *Smart Mater. Struct.*, vol. 21, no. 9, 2012, doi: 10.1088/0964-1726/21/9/094016.

[16] D. J. Hartl, D. C. Lagoudas, F. T. Calkins, and J. H. Mabe, "Use of a Ni60Ti shape memory alloy for active jet engine chevron application: I. thermomechanical characterization," *Smart Mater. Struct.*, vol. 19, no. 1, 2010, doi: 10.1088/0964-1726/19/1/015020.

[17] D. J. Hartl, J. T. Mooney, D. C. Lagoudas, F. T. Calkins, and J. H. Mabe, "Use of a Ni60Ti shape memory alloy for active jet engine chevron application: II. Experimentally validated numerical analysis," *Smart Mater. Struct.*, vol. 19, no. 1, 2010, doi: 10.1088/0964-1726/19/1/015021.

[18] A. Y. N. Sofla, S. A. Meguid, K. T. Tan, and W. K. Yeo, "Shape morphing of aircraft wing: Status and challenges," *Mater. Des.*, vol. 31, no. 3, pp. 1284–1292, 2010, doi: 10.1016/j.matdes.2009.09.011.

[19] U. Icardi and L. Ferrero, "Preliminary study of an adaptive wing with shape memory alloy torsion actuators," *Mater. Des.*, vol. 30, no. 10, pp. 4200–4210, 2009, doi: 10.1016/j.matdes.2009.04.045.

[20] O. J. Godard, M. Z. Lagoudas, and D. C. Lagoudas, "Design of space systems using shape memory alloys," *Smart Struct. Mater. 2003 Smart Struct. Integr. Syst.*, vol. 5056, p. 545, 2003, doi: 10.1117/12.483469.

[21] B. Huettl and C. E. Willey, "Design and development of miniature mechanisms for small spacecraft," *14th AIAA/USU Conf. Small Satelites*, pp. 1–14, 2000.

[22] A. D. Johnson, "Non-Explosive Separation Device," *United State Patent*, Patent No. 5119555, 1992.

[23] General Motor, "Lightweight smart material on corvette," *General Motors News*, 2013 [Online] Available: https://media.gm.com/media/us/en/gm/home.detail.html/content/Pages/news/us/en/2013/Feb/0212-corvette.html.

[24] A. L. Browne *et al.*, "SMA heat engines : Advancing from a scientific curiosity," *SMART Mater. Struct. NDT Aerosp. Conf.*, 2-4 November 2011, Quebec, Canada.

[25] R. DesRoches, J. McCormick, and D. M., "Cyclical properties of superelastic shape memory alloys," *ASCE J. Struct. Eng.*, vol. 130, no. 1, pp. 38–46, 2004.

[26] J. Leng, X. Yan, X. Zhang, D. Huang, and Z. Gao, "Design of a novel flexible shape memory alloy actuator with multilayer tubular structure for easy integration into a confined space," *Smart Mater. Struct.*, vol. 25, no. 2, 2016, doi: 10.1088/0964-1726/25/2/025007.

[27] D. Singh, R. Choudhury, Y. Singh, and M. Mukherjee, "Workspace analysis of 3-DOF U-shape base planar parallel robotic motion stage using shape memory alloy restoration technique (SMART) linear actuators," *SN Appl. Sci.*, vol. 3, no. 4, pp. 1–22, 2021, doi: 10.1007/s42452-021-04490-y.

[28] D. Singh, R. Choudhury, Y. Singh, and M. Mukherjee, "Development and workspace analysis of smart actuation based planar parallel robotic motion stage," *IOP Conf. Ser. Mater. Sci. Eng.*, vol. 912, no. 3, 2020, doi: 10.1088/1757-899X/912/3/032063.

[29] D. Singh, Y. Singh, and M. Mukherjee, "Behaviour of NiTi based smart actuator for the development of planar parallel micro-motion stage," *Adv. Mech. Eng.*, pp. 221–228, 2021.

[30] F. Auricchio, "A robust integration-algorithm for a finite-strain shape-memory-alloy superelastic model," *Int. J. Plast.*, vol. 17, no. 7, pp. 971–990, 2001, doi: 10.1016/S0749-6419(00)00050-4.

[31] F. Auricchio, D. Fugazza, and R. DesRoches, "Numerical and experimental evaluation of the damping properties of shape-memory alloys," *J. Eng. Mater. Technol. Trans. ASME*, vol. 128, no. 3, pp. 312–319, 2006, doi: 10.1115/1.2204948.